COMMUNICATION

Check for updates

Piezoelectric PVDF membranes for emulsion separation with constant flux and high efficiency†

Xin Zhong[a] and Zhiguang Guo ⓘ *[ab]

Emulsion separation, a focal and challenging aspect of oil−water separation processes, has long been a source of frustration for researchers due to the phenomenon of flux decline caused by concentration polarization and adhesion of oil droplets during the separation process. Attempts have been made to address membrane fouling issues through catalytic degradation and bubble flotation methods; however, the flux decline phenomenon persisted. In this work, during the fabrication process, intermolecular forces were utilized to polarize polyvinylidene difluoride molecular chains to increase the β-phase and endow them with piezoelectric properties. The prepared piezoelectric membrane, under the variable pressure environment created using a peristaltic pump, could maintain stable flux throughout the separation process without decline while maintaining high separation efficiency, as opposed to constant pressure filtration. It was found that the main mechanism of action was dielectrophoretic forces, and the feasibility was theoretically analyzed, showing promise for the extension to the separation of a greater variety of oil-in-water emulsions. Additionally, the piezoelectric catalytic effect could generate reactive oxygen species, which could further degrade organic pollutants to alleviate membrane surface contamination and blockage, further maintaining flux. This work provides new insights into the development of emulsion separation applications.

New concepts

Piezoelectric PVDF membranes were prepared by the synergistic pulling of DA/SA through the NIPS method, with a simple preparation process and no additional post-processing steps, which is conducive to industrial preparation. It was found that the piezoelectric effect can achieve nearly constant flux while maintaining high separation efficiency during the emulsion separation process, and the feasibility of dielectrophoretic forces for the separation of other oily substances was theoretically analyzed. Organic pollutants can be degraded through piezoelectric catalysis, further reducing the accumulation of membrane surface pollution and aiding the separation process.

1. Introduction

The global annual output of oily wastewater is about 1.0×10^{10}–1.5×10^{10} m^3. A large amount of oily wastewater discharged into nature or a single entity of population results not only in a loss of energy, but also in destruction and damage to the ecological environment and human life and health. Separation and recycling are the main solutions.[1,2] For the most challenging part of oil–water separation—emulsion separation, membrane separation is the method most frequently employed by researchers at present.[3–6] During the separation process, oil droplets exhibit behaviors such as adhesion, pinning, wetting, diffusion, plugging, intrusion, coalescence, and separation on the membrane surface.[7]

Moreover, due to the filtration of target substances and the interception of unwanted materials, it is inevitable that unfiltered substances accumulate on the membrane surface, leading to an increase in their concentration at the membrane surface and a consequent decrease in flux. During the separation of water-in-oil emulsions, this concentration polarization and accumulation of substances increase the probability of oil adhering to the membrane surface, promoting the adhesion of oily contaminants on the membrane surface or within the membrane pores.[8] This leads to a continuous decrease in flux during the separation process as the separation time increases. Typically, cleaning operations are performed after each separation to restore flux, but this can only remove reversible fouling. It is ineffective in dealing with irreversible fouling that adheres within the membrane pores.

Researchers used cross-flow filtration,[9] rotating separation membranes,[10] catalytic degradation,[11,12] bubble-mediated,[13–15] electrophoretic forces,[16] and other methods to reduce oil

[a] Ministry of Education Key Laboratory for the Green Preparation and Application of Functional Materials, Hubei University, Wuhan 430000, People's Republic of China. E-mail: zguo@licp.cas.cn; Fax: +86-931-8277088; Tel: +86-931-4968105
[b] State Key Laboratory of Solid Lubrication, Lanzhou Institute of Chemical Physics, Chinese Academy of Sciences, Lanzhou 730000, People's Republic of China
† Electronic supplementary information (ESI) available. See DOI: https://doi.org/10.1039/d5nh00298b

pollution and reduce the flow reduction caused by oil plugging. But these are only slowdowns, and flux decay is inevitable during the separation process. Dai et al.[17] reported that the emulsion separation was carried out using a non-contact ion air device, but the separation efficiency was low and the energy consumption was high. Liu et al.[18] used a non-filter separation, by rotating the separation device contact with the selection of oil and water for synchronous separation. But this gear opening and closing in the use of the process also causes mechanical wear.

Some researchers have found that the piezoelectric effect in the emulsion separation for oil pollution discharge plays an effective role. The piezoelectric effect refers to the ability of materials to convert mechanical energy into electrical energy during vibration, which is divided into the direct piezoelectric effect and the converse piezoelectric effect. Both of these can be effectively used for emulsion separation. Regarding the converse piezoelectric effect, when an alternating voltage is applied to the material, it undergoes internal contractions that generate inherent ultrasound and vibrations. Piezoelectric vibration can reduce the filtration resistance caused by concentration polarization and membrane fouling, thereby producing a self-cleaning effect.[19] Cao et al.[20] prepared a piezoelectric polyvinylidene difluoride (PVDF) membrane through the thermally induced phase separation method combined with high-pressure polarization treatment. It was found that applying alternating current of a given frequency to the membrane could generate in situ vibrations to reduce membrane fouling. The water flux through the piezoelectric membrane increased with the increase in alternating current, increasing by 72.6% (20 V) compared to the membrane without the application of alternating current. The highest water flux was achieved at a frequency of 10 kHz. Pu et al.[19] also designed a piezoelectric PVDF membrane, and reported that the reduction in the concentration polarization layer and membrane fouling due to piezoelectric vibration were the reasons for the increase in membrane flux. In addition, it was demonstrated that the piezoelectric vibration was effective against different charged foulants. However, when using the converse piezoelectric effect for emulsion separation, there is still an initial stage where flux decline occurs.[21] The direct piezoelectric effect demonstrates greater advantages in emulsion

separation.[22] The piezoelectric membrane generates current pulses and rapid voltage oscillations through transient water pressure fluctuations across the membrane, while also producing reactive oxygen species (ROS) through piezoelectric catalysis, exhibiting anti-fouling effects against a range of membrane contaminants including organic molecules, oil droplets, proteins, bacteria, and inorganic colloids.[23–25] Additionally, the peristaltic pump device that provides a variable pressure environment is more in line with industrial application settings, facilitating the promotion and application of piezoelectric membrane separation.

PVDF is frequently used for emulsion separation due to its production cost and excellent chemical and thermal stabilities. Additionally, its asymmetric molecular structure allows for the fabrication of flexible films with piezoelectric effects. Generally, electrospinning is employed for the polarization preparation of piezoelectric PVDF.[26–30] Alternatively, the content of polar phases in PVDF can be increased through thermocompression and electrostatic interactions between positively and negatively charged films on different surfaces.[31] However, from an industrial manufacturing perspective, solution casting has more advantages. However, the rapid phase separation of water and irregular flow limit self-polarization. After the application of a polarizing force, the polymer chains in the thin film can slowly align, aiding the internal arrangement of the amorphous β-phase, thereby generating a piezoelectric response.[32] In this work, dopamine hydrochloride (DA) and sodium alginate (SA) were used to apply polarizing forces to promote the polarization of molecular chains.[33,34] Using 1-methyl-2-pyrrolidinone (NMP) as a polar solvent, compared to other solvents, it has superiority in preparing a high β-phase through the non-solvent induced phase separation (NIPS) method. Moreover, a low-temperature bath and a long soaking time are conducive to the formation of the β-phase.[35] The prepared membrane (PDS-1) and the control samples (PVDF-DA, PVDF-SA, and PDS-2) were subjected to a series of characterization studies to verify the feasibility of stretch polarization, followed by emulsion separation tests and piezoelectric catalysis experiments to explore the application of the direct piezoelectric effect in emulsion separation.

Miss Xin Zhong joined Prof. Guo's biomimetic materials of tribology (BMT) group at Hubei University in 2022 to pursue her PhD degree. Her current scientific interests are focused on PVDF membranes for separation.

Xin Zhong

Professor Zhiguang GUO is a full professor and Dean of the School of Materials Science and Engineering, Hubei University. He has published more than 620 papers on the interfaces of materials, and his H index is 87.

Zhiguang Guo

2. Results and discussion

2.1. Fabrication of PDS-1

The directional alignment of CH_2–CF_2 units to form the all-trans chain conformation (TTTT, β phase) is beneficial for enhancing the piezoelectric performance of PVDF. Therein, augmenting intermolecular interactions during the molding process can effectively polarize PVDF.[36] Upon contact with water in the solvent bath, the carboxyl and hydroxyl groups of sodium alginate form hydrogen bonds with water molecules, leading to the dissociation of sodium alginate molecules and imparting a negative charge characteristic to its aqueous solution.[37] The anionic groups of SA interact with the –CH_2 of PVDF. In the casting solution, the –$H^{\delta+}$ from the amino and hydroxyl groups in DA can form strong interactions, specifically hydrogen bonds, with the –$F^{\delta-}$ in –CF_2.[38] The anionic groups of alginate and DA exhibit ion–dipole and hydrogen bond–dipole interactions with different sides of PVDF, respectively, which facilitate the directional alignment and polarization of PVDF molecular chains during the molding process, thereby increasing the content of the β-phase (Fig. 1a).[39] The morphology of PVDF powder before molding and the surface of the PVDF membrane after molding were characterized using a field emission scanning electron microscope (Fig. S1, ESI†). For the raw material PVDF powder, it exhibits a spherical shape, indicating a thermodynamically stable state formed by the free aggregation of PVDF molecular chains. After dissolution in a polar solvent, PVDF chains will extend and entangle with other molecular chains to form a shape. Due to the solvent exchange rate and the mode of action of additives, PVDF films exhibit different characteristics. Regarding the morphology after film formation, it was found that the bottom of the film (close to the glass plate side) exhibits a porous morphology with a porosity of about 13%, and the pore size ranges from 0.1 to 1.7 μm. The top of the film shows a dense morphology with small pores (Fig. 1b and c). The top is in direct contact with the non-solvent; at this time, the solvent rapidly diffuses into the non-solvent, resulting in a rapid increase in the polymer concentration, resulting in rapid phase separation, allowing the polymer rich phase to rapidly cure with the poor phase, and the polymer poor phase to be separated from the polymer rich phase, and the growth of pores is limited, resulting in the formation of pores. For the removal of nanoscale oil droplets in emulsion separation, the existence of smaller pores is beneficial to increase the selectivity in the separation process. Moreover, the cross-sectional view reveals that PVDF has large and straight finger-like pore areas, further enhancing the permeation of the solution (Fig. 1d). The prepared PDS-1 exhibits hydrophilicity and achieves a water flux of up to 117 L h^{-1} m^{-2} under 0.1 bar (Fig. S2 and S3, ESI†). Energy dispersive spectroscopy was used to investigate the elemental distribution on the membrane surface, showing a uniform distribution of C, F, O, and N elements, indicating that DA and SA are uniformly distributed in PVDF during the molding process (Fig. 1e). X-ray photoelectron spectroscopy (XPS) also characterized this point; in the XPS spectrum of PDS-1, there are peaks of a small amount of O and N elements, again proving the presence of these two elements in the material, indicating the successful modification of the modifying substances (Fig. 1f).

2.2. Piezoelectric property testing

To confirm that the interactive forces between additives in the casting solution and the solvent in the solvent bath with PVDF molecular chains can polarize PVDF and increase the content of the β-phase during the molding process, the β-phase content of PVDF was characterized using Fourier transform infrared spectroscopy (FT-IR), X-ray diffraction (XRD), and Raman spectroscopy. Additionally, control samples of PVDF (without DA and the non-solvent is the deionized water, Fig. S4, ESI†), PVDF-DA (the non-solvent is the deionized water, Fig. S5, ESI†), PVDF-SA (without DA, Fig. S6, ESI†), and PDS-2 (DA content increased, Fig. S7, ESI†) were prepared to substantiate the effectiveness. From the FT-IR, the original PVDF powder's infrared peaks include those of the α-phase at 764, 880, 976, and 1186 cm^{-1}, as well as those of the β-phase at 840 and 1280 cm^{-1}. The spectrum predominantly shows the thermodynamically stable α-phase (Fig. S8a, ESI†). After interaction and pulling by NIPS combined with DA/SA, the intensity of the composite peak at 840 cm^{-1} for β/γ and the characteristic peak at 1275 cm^{-1} for the β-phase increased, while the intensity of the peak at 766 cm^{-1}, indicative of the α-phase, decreased, indicating an increase in the β-phase content of the molded film (Fig. 2a). Comparing with the FT-IR of the PVDF, it was found that the presence of DA or SA alone can slightly increase the content of the β-phase (Fig. S8b, ESI†). However, their ability to pull the PVDF molecular chains into the high-energy β-phase is still insufficient, and the synergistic effect of both is better. When the content of DA is increased, the characteristic peak of the β-phase at 1275 cm^{-1} weakens, indicating that the content of the β-phase decreases with further increase in DA, suggesting that there is an optimal addition value for fillers to increase the β-phase content in PVDF. The content of the β-phase was quantitatively substantiated by calculating it using the Lambert–Beer law formula, which numerically corroborated the changes in the β-phase (Fig. 2b).[40] The PDS-1 membrane, with PVDF molecular chains synergistically pulled by DA/SA, has a β-phase content as high as 82.3%, which is higher than that of the control samples with single pulling and increased DA content (for PVDF membranes, $F(\beta)$ was 57.5%), matching the changes in the infrared peak intensities. XRD was used to further determine the changes in the β-phase content by examining the different diffraction peak positions and corresponding peak intensities for different crystalline phases. For the original PVDF powder, the main diffraction peaks are at 17.7°, 18.4°, 20.0°, and 26.7°, corresponding to the α-phase (100), (020), (110), and (120) crystal planes, indicating that the freely aggregated PVDF molecular chains primarily exhibit the thermodynamically stable α-phase (Fig. S9a, ESI†). After the film formation, the PVDF membrane exhibited a weaker β-phase crystalline peak, while PDS-1 showed essentially only one strong diffraction peak, namely 20.6° attributed to the (110)/(200) β-phase diffraction peak (Fig. S9b, ESI† and Fig. 2c). The intensity of the diffraction peaks indicates the changes in the β-phase content. PDS-1 has the strongest peak intensity, while other control samples exhibit a
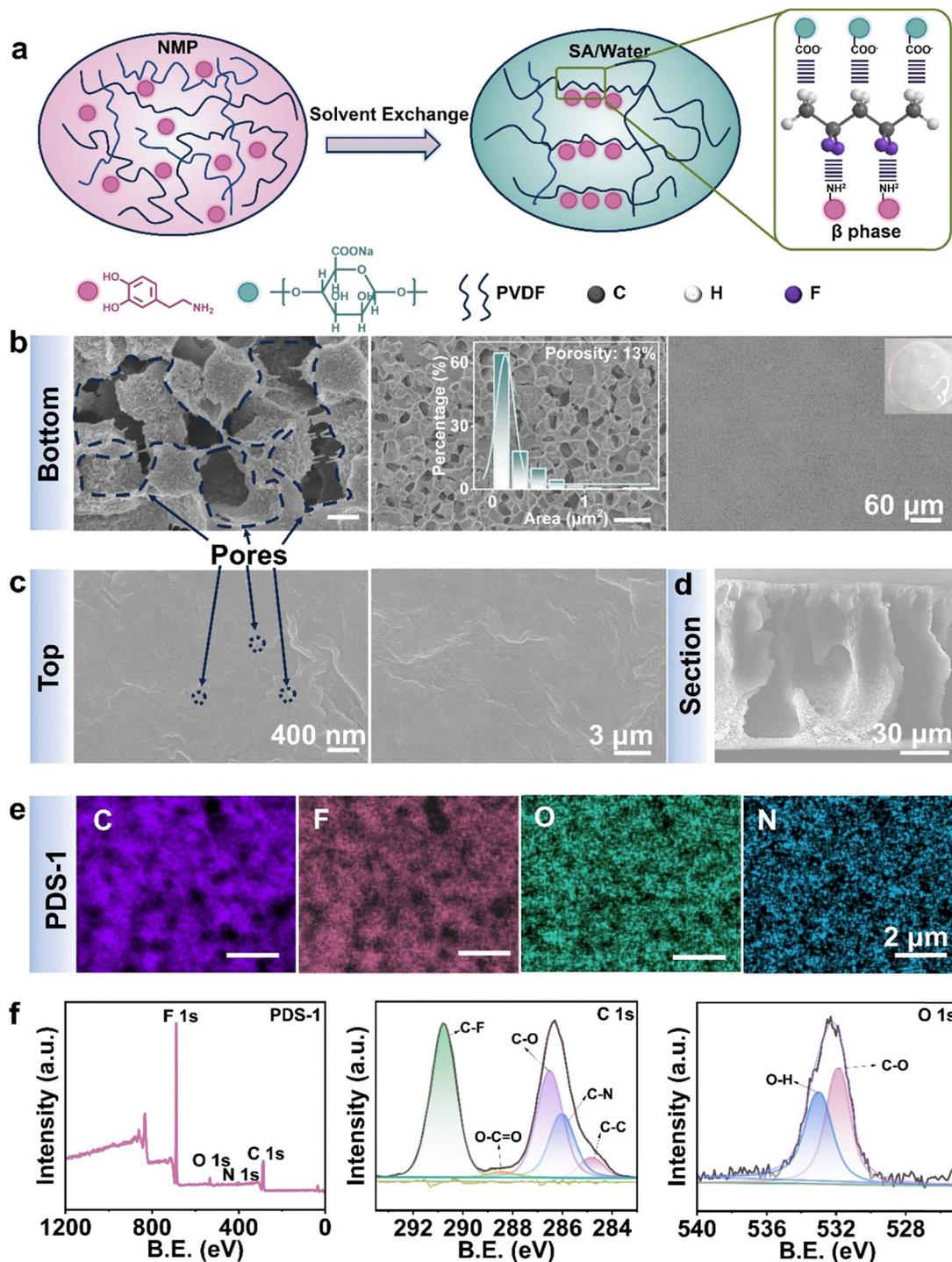
Fig. 1 (a) Schematic diagram of the chain segment movement during PVDF molding. The field emission scanning electron microscopy images of the bottom (b), top (c), and cross-section (d) of PDS-1, as well as the pore distribution map and optical photograph. (e) Energy dispersive spectroscopy mapping images of PDS-1. (f) XPS spectrum of PDS-1 and the corresponding high-resolution spectra.

slight weakening. The strong β phase diffraction peak indicates that PDS-1 has the highest β-phase content, and the trend is consistent with the infrared spectrum, further proving the feasibility of the preparation method for increasing. The peaks at 800 and 835 cm^{-1} in the Raman spectrum correspond to the α-phase/γ-phase and β-phase, respectively.[41] The Raman peak

of PDS-1 at 835 cm^{-1} shows a significant increase compared to the control samples, indicating an increase in the content of the β-phase and further proving the success of the experiment (Fig. 2d and Fig. S10, ESI†). The uniformity of the PDS-1 film was tested using Raman mapping. Fig. 2e shows the distribution of the peak at 835 cm^{-1} across the test area, and it can be
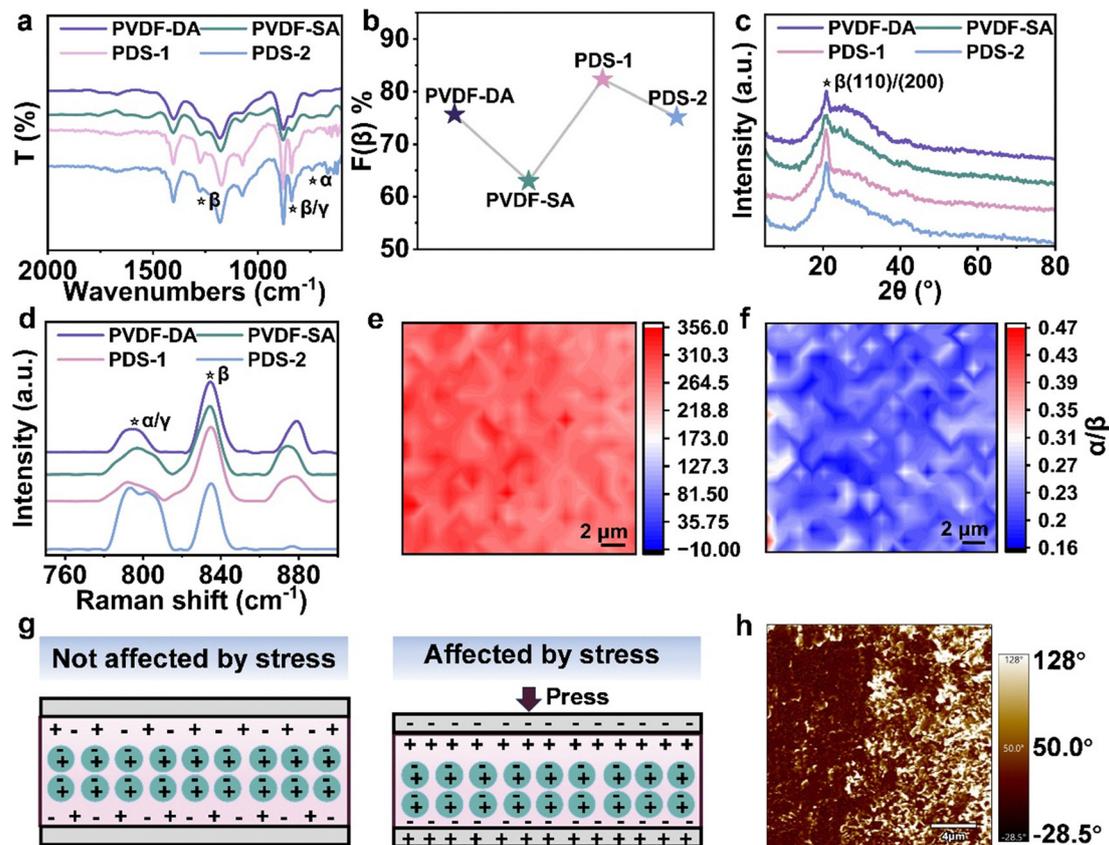
Fig. 2 FT–IR spectra (a), β-phase content (b), XRD patterns (c), and Raman spectra (d) of PVDF-DA, PVDF-SA, PDS-1, and PDS-2. Raman mapping images of PDS-1 regarding the distribution of the β-phase (e) and the ratio distribution of α/β phases (f). (g) Schematic diagram of the piezoelectric response. (h) The phase diagram of PDS-1.

observed that the color throughout the area is uniform, indicating a uniform distribution of the β-phase. Fig. 2f shows the distribution of the ratio of α/β phases; a tendency towards red indicates an increase in the content of the α-phase, while a tendency towards blue indicates that the β-phase is the main component. It can be seen that the entire area is predominantly the β-phase, further indicating that the preparation method helps to arrange the molecular chains in a β-phase manner, enhancing the asymmetry of the material.

For materials with asymmetric structures, the application of mechanical forces causes a shift in the polarity of the electric field within their non-centrosymmetric structures, leading to the displacement of positive and negative charges and the electrification of the material surface (Fig. 2g).[24] PVDF, due to the asymmetric structure of $CH_2–CF_2$, has the potential for piezoelectric performance, and typically increasing the β-phase of PVDF can enhance the material's piezoelectric properties. It has been confirmed that ion–dipole interactions and hydrogen bond–dipole interactions can effectively increase the content of the β-phase in PVDF. The piezoelectric properties of the samples were tested using piezoresponse force microscopy (Fig. 2h and Fig. S11, S12, ESI†). Fig. 2h shows the phase image of PDS-1. It can be observed that PDS-1 exhibits a phase image with distinct light and dark contrasts, indicating the presence of

domains with different polarization directions, which suggests that PDS-1 has piezoelectric properties.

2.3. Emulsion separation testing

The piezoelectric effect of PVDF is stimulated when it experiences varying mechanical forces, and conventional dead-end filtration used for emulsion separation cannot generate a piezoelectric response in PVDF due to the separation pressure being essentially constant. Therefore, to stimulate the piezoelectric effect for emulsion separation, a peristaltic pump separation method is employed (Fig. 3a). By dead-end filtering emulsions containing three different types of surfactants, it was found that, consistent with the results of most researchers, due to concentration polarization and material accumulation, the separation flux gradually decreases with increasing separation time (Fig. 3b, c and Fig. S13, ESI†). In terms of efficiency, the emulsion containing Tween 80 surfactant had the best efficiency, reaching 99.5%. The separation efficiencies for sodium dodecyl sulfate (SDS) and hexadecyl trimethyl ammonium bromide (CTAB) were relatively lower, at 96.9% and 98.7%, respectively. The reduction in efficiency is attributed to the smallest particle size of the SDS emulsion, which is more likely to pass through the pores. CTAB is a cationic surfactant, the PVDF film surface tends to carry a negative charge due to the

presence of CF$_2$, and the sodium alginate solution, acting as a solvent bath, coats the PVDF surface. The alginate anions also impart a negative charge to the PDS-1 film after membrane formation, leading to a decrease in efficiency due to the attraction with the cationic surfactant. Compared with the PVDF separating emulsion with Tween 80 as the surfactant under atmospheric pressure, PDS-1 has a small increase in flux and separation efficiency (the separation efficiency of the PVDF membrane is 99.3%), indicating that the addition of DA and SA results in a limited improvement in the separation effect of the membrane under atmospheric pressure (Fig. S14a, ESI†). In emulsion separation experiments powered using a peristaltic pump, it can be observed that the flux does not decrease with the increase of time, but rather remains essentially constant (Fig. 3d and Fig. S15, ESI†). The separation effect of PDS-1 through pressure variation separation is slightly lower compared to the constant pressure separation, but it still remains a relatively high level overall. For Tween 80, the efficiency can reach up to 98.8%, and both SDS and CTAB are above 96%. In contrast to PVDF with a low β-phase, which separates Tween 80–surfactant emulsions at variable pressures, PVDF exhibits unstable undulating flux when separating unstained emulsions, and the separation efficiency decreased to 96.5%. The decrease in separation efficiency is due to the low β phase PVDF membrane for pollutant removal ability is weak, and the accumulation of oil under the action of pressure to increase the probability of passing through the membrane (Fig. S14b, ESI†). However, when the dyeing emulsion is separated, the pollutants increase to be oil and dye, and the PVDF of the low β phase has a weak ability to remove it, which leads to the rapid accumulation of pollutants on the membrane surface. The separation efficiency of PVDF is lower than 63.3% at 15 min due to the separation failure caused by the sudden increase of the pressure inside the membrane tank (Fig. S14c, ESI†). The PDS-1 membrane with the high β phase can stably separate the dyed emulsion, indicating that the piezoelectric effect can effectively remove pollutants, thus ensuring the stability of flux and high separation efficiency. Moreover, the separation of emulsions with different charged types showed stable flux and efficient separation, which indicated that the main reason for the alleviation of concentration polarization and material accumulation was not the electrophoretic force, but another mechanism. To rule out the possibility that the non-declining flux is due to a mismatch between the flow rate and separation flux leading to increased pressure, it was found that even when the flow rate is reduced, the flux remains constant throughout the separation process, indicating that it is not due to pressure effects (Fig. 3e and Fig. S16, ESI†).

Porous piezoelectric surfaces convert an absorbed mechanical force into an electric field, which is a non-uniform electric field. This non-uniform electric field can generate dielectrophoretic forces (DEP) on particles within the field. These forces are independent of the type of charge on the particles and are related to the particles' dielectric constants and sizes. The magnitude of DEP on particles in the electric field is calculated using eqn (1):

$$F_{DEP} = 2\pi r_e^3 \epsilon_m R_e[\underline{Ke}] \nabla |E_{rms}|^2 \qquad (1)$$

where r_e represents the radius of a spherical particle, and ϵ_m denotes the dielectric constant of the medium. $R_e[\underline{Ke}]$ is the real part of the Clausius–Mossotti factor, ∇ is the del vector, and $|E_{rms}|^2$ is the squared electric field intensity, which is equal to $E_p^2/2$. $R_e[\underline{Ke}]$ can be expressed as eqn (2):

$$R_e[\underline{Ke}] = \frac{\epsilon_p - \epsilon_m}{\epsilon_p + 2\epsilon_m} + \frac{3(\epsilon_m\sigma_p - \epsilon_p\sigma_m)}{\tau(\sigma_p + 2\sigma_m)^2(1 + \omega^2\tau^2)} \qquad (2)$$

where ϵ_p, σ_p, and σ_m represent the dielectric constant, conductivity of the particles, and the conductivity of the medium, respectively. ω is the angular frequency (= $2\pi f$). τ denotes $(\epsilon_p + 2\epsilon_m)/(\sigma_p + 2\sigma_m)$. Therefore, $R_e[\underline{Ke}]$ can be rewritten as eqn (3):

$$R_e[\underline{Ke}] = \frac{(\epsilon_p - \epsilon_m)\omega^2\tau^2}{(\epsilon_p + 2\epsilon_m)(1 + \omega^2\tau^2)} + \frac{(\sigma_p - \sigma_m)}{(\sigma_p + 2\sigma_m)(1 + \omega^2\tau^2)} \qquad (3)$$

when $\omega < 1/\tau$, $R_e[\underline{Ke}]$ is mainly controlled by σ_p and σ_m; when $\omega > 1/\tau$, $R_e[\underline{Ke}]$ is mainly controlled by ϵ_p and ϵ_m.[42] When $R_e[\underline{Ke}]$ is positive, droplets are attracted to regions of high electric field strength (positive dielectrophoresis), and when $R_e[\underline{Ke}]$ is negative, droplets move away from regions of high electric field strength (negative dielectrophoresis).[43] For the separated toluene emulsion system, the main parameters are as follows (Table 1):

At this point, the value of τ is approximately 1.4×10^7, and the $1/\tau$ value is approximately 6.9×10^{-8}. Therefore, essentially, within a broad frequency range for the toluene emulsion system, the value of $R_e[\underline{Ke}]$ is related to the dielectric constants of the droplets and the medium within the system. And since $\epsilon_p < \epsilon_m$ and $\sigma_p < \sigma_m$, $R_e[\underline{Ke}]$ will be negative across the entire frequency range. For the entire separation system, the PDS-1 membrane acts as a region of high electric field strength, so the oil droplets in the emulsion will move away from the membrane. This DEP effectively reduces the concentration polarization and material accumulation on the membrane surface, allowing the separation flux to be maintained at a certain value (Fig. 3f). Moreover, since the dielectric constants and conductivities of most oil droplets are lower than that of water, this mechanism can be applied to the separation of most oil–water emulsions (Fig. 3g).

2.4. ROS testing

Piezoelectric materials can collect mechanical energy and then convert it into electrical energy. During the piezoelectric conversion process, electrons and holes generated on the membrane surface can react with substances such as water and oxygen in the environment to produce ROS. ROS can be used to degrade organic pollutants (Fig. 4a). Through dye degradation experiments, the ability of ROS to degrade organic substances was investigated. The PDS-1 membrane, cut into pieces of 1.5 × 1.5 cm, was immersed in a methylene blue solution. Before the experiment began, the methylene blue solution was sonicated for 0.5 h without the PDS-1 membrane, and it was found that the concentration did not decrease significantly, indicating that sonication alone does not lead to the degradation of methylene blue. The piezoelectric PVDF
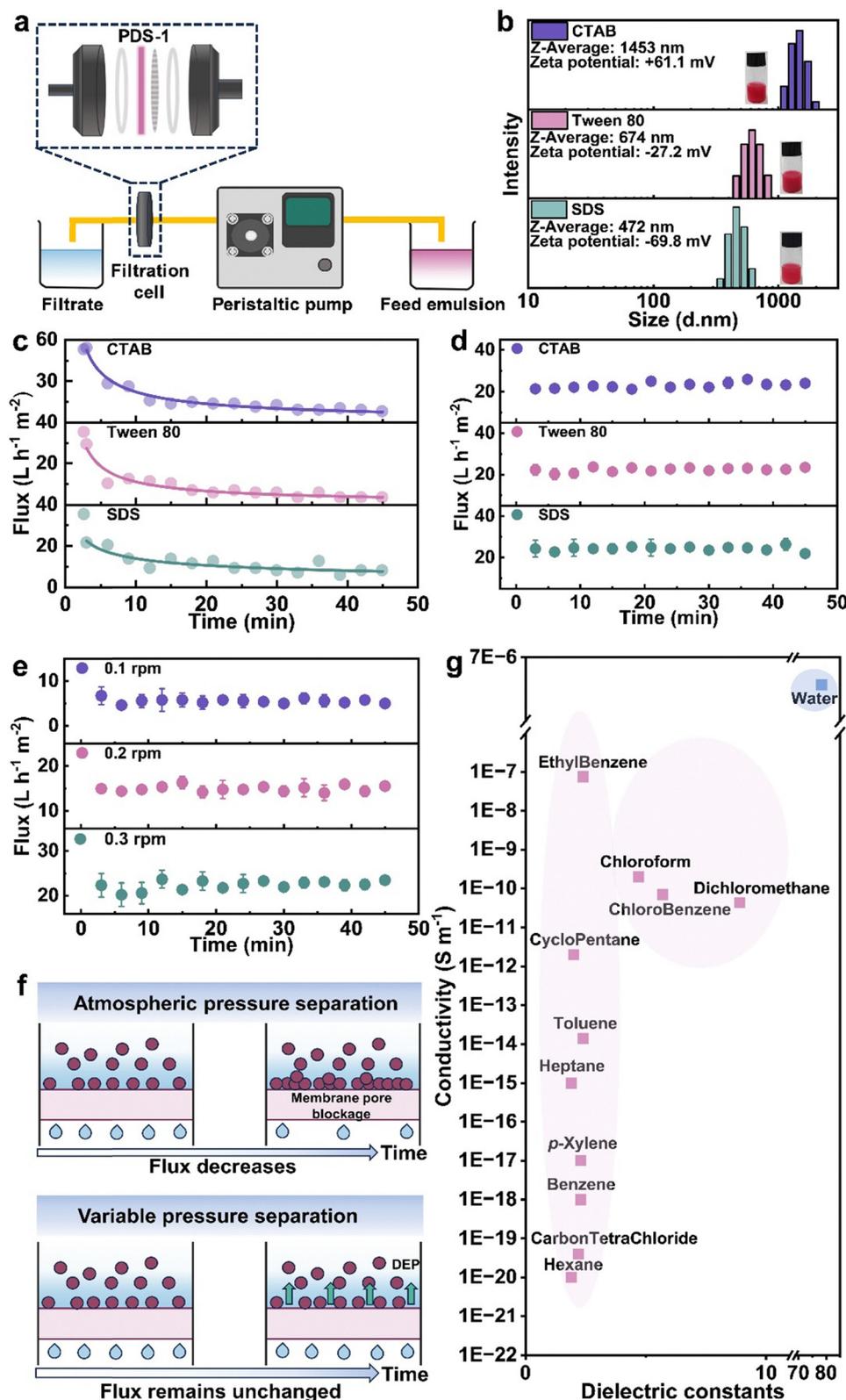
Fig. 3 (a) Schematic diagram of the peristaltic pump separation device. (b) Particle size distribution and zeta potential of the emulsions containing CTAB, Tween 80, and SDS surfactants. Variation of separation flux with time for PDS-1 under atmospheric pressure (c) and variable pressure (d) for three different emulsions. (e) Variable pressure emulsion separation by PDS-1 at different rotation speeds. (f) Schematic diagram of the mechanisms for separation under atmospheric pressure and variable pressure. (g) Conductivity and dielectric constants of common oil substances used for emulsion separation compared to water.

Table 1 The electrical conductivity and dielectric constants of the various components in the toluene emulsion system

Components	σ (S m^{-1})	ϵ
Particles (toluene)	1.4×10^{-14}	2.3741
Medium (water)	5.5×10^{-6}	78.3553

membrane was then added, and adsorption–desorption was conducted in a dark environment for 2 h, with tests performed every hour. After 2 h, the concentration remained essentially unchanged, indicating that adsorption–desorption equilibrium was reached. Subsequently, ultrasonic vibration was applied to promote the generation of ROS for dye degradation experiments, with tests conducted every 15 min. It was observed that the concentration of methylene blue consistently decreased with the increase in sonication time, demonstrating that ultrasonic vibration can induce the piezoelectric PVDF to produce ROS, thereby promoting dye degradation (Fig. 4b and c). This indirectly proves the generation of ROS and its ability to

degrade organic substances, which is beneficial for the anti-fouling performance of the piezoelectric PVDF membrane during separation. The generation of ROS was demonstrated by capturing free radicals using fluorescent reagents and detecting the fluorescence produced. The fluorescence spectrum was measured with a one-minute interval for each detection. It was found that with each minute of vertexing, the PDS-1 membrane, by obtaining mechanical forces, causes the electrons and holes on its surface to react with water and oxygen to produce free radicals, which is reflected in the increase in fluorescence intensity, thereby confirming the generation of ROS (Fig. 4d). Furthermore, fluorescence signals were directly observed using a fluorescence confocal microscope, showing that fluorescence was uniformly generated both in the solution and on the surface of the PDS-1 membrane, indicating that the ROS generated by PDS-1 is evenly distributed in the solution (Fig. 4e). The generation of hydroxyl radicals and superoxide radicals under vibration conditions was also demonstrated (Fig. S17, ESI†).
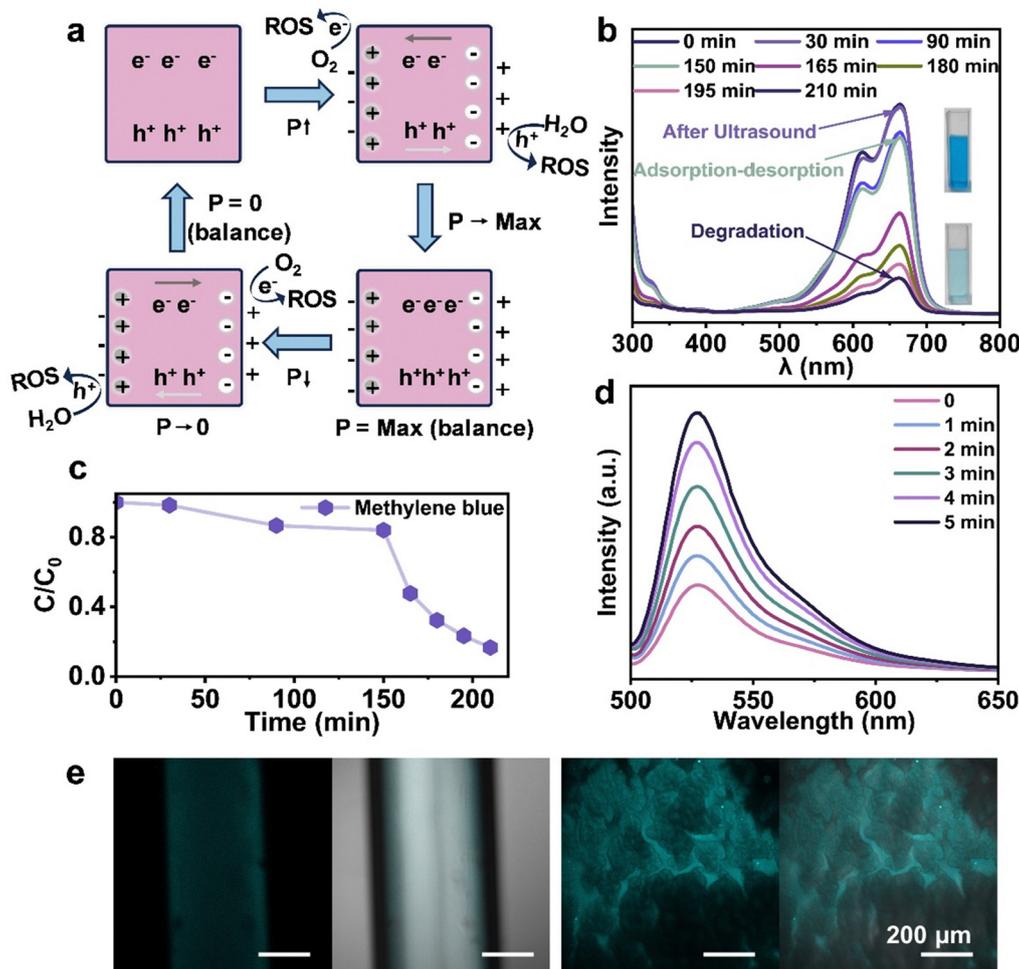

Fig. 4 (a) Schematic illustration of piezoelectric catalysis. Ultrasonic degradation experiment of the methylene blue dye by PDS-1 (b) and the degradation curve (c). (d) Fluorescence spectrum regarding the generation of ROS. (e) Fluorescence images of ROS in the solution and on the surface of PDS-1.

3. Conclusions

PDS-1 membranes with different pore distributions were prepared by the NIPS method. During the film formation process, additives and non-solvents promoted the β-phase arrangement of PVDF molecular chains through ion–dipole and hydrogen bond–dipole interactions. The increase in the β-phase was confirmed by FT-IR, XRD, and Raman characterization methods, and the piezoelectric effect of PDS-1 was demonstrated by the polarization domains using piezoresponse force microscopy. The emulsion separation of PDS-1 under atmospheric pressure and variable pressure was compared, with the separation under atmospheric pressure showing a gradual decline in flux over separation time, similar to most researchers' findings. In contrast, pressure swing separation experiments using a peristaltic pump showed that PDS-1 maintains efficient and stable separation throughout the separation process. The mechanism's feasibility was confirmed by calculating the dielectrophoretic force, and it is expected to be applicable to the separation of most oil–water emulsions. Additionally, the piezoelectric effect can lead to the generation of ROS, which can be used to degrade organic pollutants, further reducing membrane surface pollution, blockage, and accumulation to maintain flux.

Conflicts of interest

The authors declare no conflicts of interest/competing interests.

Data availability

The authors declare that all data in this manuscript are available upon reasonable request.

Acknowledgements

References

1 Y. Gu, Q. Xia, B. Liu, Y. Zhao, L. Pu, J. Ding, Y. Liu, E. Li, C. D. Vecitis and G. Gao, Electric Demulsification Membrane Technology for Confined Separation of Oil–Water Emulsions, *Environ. Sci. Technol.*, 2024, **58**(45), 20277–20288, DOI: **10.1021/acs.est.4c06566**.

2 Y. Zhao, Y. Gu and G. Gao, Piezoelectricity Induced by Pulsed Hydraulic Pressure Enables in Situ Membrane Demulsification and Oil/water Separation, *Water Res.*, 2022, **215**, 118245, DOI: **10.1016/j.watres.2022.118245**.

3 A. Hai, A. A. Durrani, M. Selvaraj, F. Banat and M. A. Haija, Oil-water Emulsion Separation Using Intrinsically Superoleophilic and Superhydrophobic PVDF Membrane, *Sep. Purif. Technol.*, 2019, **212**, 388–395, DOI: **10.1016/j.seppur.2018.10.001**.

4 C. Chen, L. Chen, D. Weng, S. Chen, J. Liu and J. Wang, Revealing the Mechanism of Superwetting Fibrous Membranes for Separating Surfactant-free Water-in-oil Emulsions, *Sep. Purif. Technol.*, 2022, **288**, 120621, DOI: **10.1016/j.seppur.2022.120621**.

5 Y.-X. Wang, Y.-J. Li, H. Yang and Z.-L. Xu, Super-wetting, Photoactive TiO2 Coating on Amino-silane Modified PAN Nanofiber Membranes for High Efficient Oil-water Emulsion, *Sep. Appl., J. Membr. Sci.*, 2019, **580**, 40–48, DOI: **10.1016/j.memsci.2019.02.062**.

6 Y. Hu, X. Lin, D. Liu, L. Liang, C. Pang, X. Pan and H. Wang, Electrospun Polymethyl Methacrylate Fibers-based Membrane with Heterogeneous Structure Achieving a Full-particle Size Separation of Oil-water Emulsion, *J. Membr. Sci.*, 2023, **680**, 121716, DOI: **10.1016/j.memsci.2023.121716**.

7 J. Zhang, K. Peng, Z.-K. Xu, Y. Xiong, J. Liu, C. Cai, X. Huang and A. Comprehensive, Review on the Behavior and Evolution of Oil Droplets During Oil/water Separation by Membranes, *Adv. Colloid Interface Sci.*, 2023, **319**, 102971, DOI: **10.1016/j.cis.2023.102971**.

8 M. Manouchehri and A. Comprehensive, Review on State-of-the-art Antifouling Super(wetting and anti-wetting) Membranes for Oily Wastewater Treatment, *Adv. Colloid Interface Sci.*, 2024, **323**, 103073, DOI: **10.1016/j.cis.2023.103073**.

9 Y. Zhao, Y. Tan, F.-S. Wong, A. G. Fane and N. Xu, Formation of Dynamic Membranes for Oily Water Separation by Crossflow Filtration, *Sep. Purif. Technol.*, 2005, **44**(3), 212–220, DOI: **10.1016/j.seppur.2005.01.010**.

10 Y. Yang, G. Liu, H. Liu, Q. Wang, Y. Wang, J.-E. Zhou and Q. Chang, Separation of Oil–water Emulsion by Disc Ceramic Membrane under Dynamic Membrane Filtration Mode, *Sep. Purif. Technol.*, 2022, **300**, 121862, DOI: **10.1016/j.seppur.2022.121862**.

11 U. Baig, M. F. Al-Kuhaili and M. A. Dastageer, Remediation of Crude Oil Contaminated Oily Wastewater Using Nanostructured ZnO-decorated Ceramic Membrane: Membrane Fouling and Their Mitigation Using Photo-catalytic Self-cleaning Process, *Desalination*, 2025, **597**, 118333, DOI: **10.1016/j.desal.2024.118333**.

12 S. Tian, Y. Zhang, Q. Sha, X. Zhang, T. Yang, X. Yan and N. Han, PPS/TA-PEI/β-FeOOH Membranes with Powerful Photo-Fenton Self-cleaning Capability for Efficient Oil–water Emulsion Separation, *Chem. Eng. J.*, 2024, **485**, 150069, DOI: **10.1016/j.cej.2024.150069**.

13 H. Li, J. Zhang, S. Gan, X. Liu, L. Zhu, F. Xia, X. Luo and Q. Xue, Bioinspired Dynamic Antifouling of Oil-Water Separation Membrane by Bubble-Mediated Shape Morphing, *Adv. Funct. Mater.*, 2023, **33**(26), 2212582, DOI: **10.1002/adfm.202212582**.

14 X. Wei, S. Song, T. Yu, Y. Zhang, J. Li, Y. Ma, Y. Yin and J. Yang, In Situ Microbubble-mediated Strategy for Highly Efficient Anti-crude Oil-fouling Membrane with Parallel

Nanosheet Structure, *Sep. Purif. Technol.*, 2025, **357**, 130220, DOI: **10.1016/j.seppur.2024.130220**.

15 Y. Li, H. Jiang, Y. Wu, H. Zhu, Y. Liu, H. Lu, B. Liu and Q. Yang, Microbubbles Enhance Oil-in-water Emulsion Separation in Fibrous Coalescers, *Water Res.*, 2025, **268**, 122573, DOI: **10.1016/j.watres.2024.122573**.

16 X. Li, H. Lan, G. Zhang, X. Tan and H. Liu, Systematic Design of a Flow-Through Titanium Electrode-Based Device with Strong Oil Droplet Rejection Property for Superior Oil-in-Water Emulsion Separation Performance, *Environ. Sci. Technol.*, 2022, **56**(7), 4151–4161, DOI: **10.1021/acs.est.1c07403**.

17 H. Dai, L. Yang, Y. Feng, J. Sun, F. Chen, X. Luo, Z. He, X. Xu, B. Wang, X. Liu, Z. Dong and L. Jiang, Contactless Interfacial Thin-Film Breaking Caused Splash-Like Demulsification of Floating Micron Emulsions via Ionic Wind, *Adv. Funct. Mater.*, 2023, **33**(43), 2304459, DOI: **10.1002/adfm.202304459**.

18 Z. Liu, Z. Zhan, T. Shen, N. Li, C. Zhang, C. Yu, C. Li, Y. Si, L. Jiang and Z. Dong, Dual-bionic Superwetting Gears with Liquid Directional Steering for Oil-water Separation, *Nat. Commun.*, 2023, **14**, 4128, DOI: **10.1038/s41467-023-39851-1**.

19 L. Pu, J. Zhang, C. Wang, Y. Pan, Y. Zhao, Y. Bu, Q. Zhang, B. Pan and G. Gao, Membrane Cleaning Strategy via in Situ Oscillation Driven by Piezoelectricity, *J. Membr. Sci.*, 2021, **638**, 119722, DOI: **10.1016/j.memsci.2021.119722**.

20 P. Cao, J. Shi, J. Zhang, X. Wang, J. T. Jung, Z. Wang, Z. Cui and Y. M. Lee, Piezoelectric PVDF Membranes for Use in Anaerobic Membrane Bioreactor (AnMBR) and Their Antifouling, *Performance, J. Membr. Sci.*, 2020, **603**, 118037, DOI: **10.1016/j.memsci.2020.118037**.

21 Y. Zhao, F. Yang, H. Jiang and G. Gao, Piezoceramic Membrane with Built-in Ultrasound for Reactive Oxygen Species Generation and Synergistic Vibration Anti-fouling, *Nat. Commun.*, 2024, **15**, 4845, DOI: **10.1038/s41467-024-49266-1**.

22 Y. Yan, P. Zhou, Y. Zhou, W. Zhang, P. Pi, Y. Qian, X. Wen and L. Jiang, Boosting Demulsification and Antifouling Capacity of Membranes via an Enhanced Piezoelectric Effect for Sustaining Emulsion Separation, *J. Am. Chem. Soc.*, 2024, **146**(19), 13306–13316, DOI: **10.1021/jacs.4c01655**.

23 Y. Zhao, Y. Gu, B. Liu, Y. Yan, C. Shan, J. Guo, S. Zhang, C. D. Vecitis and G. Gao, Pulsed Hydraulic-pressure-responsive Self-cleaning Membrane, *Nature*, 2022, **608**, 69–73, DOI: **10.1038/s41586-022-04942-4**.

24 J. Liu, W. Qi, M. Xu, T. Thomas, S. Liu and M. Yang, Piezocatalytic Techniques in Environmental Remediation, *Angew. Chem., Int. Ed.*, 2023, **62**(5), e202213927, DOI: **10.1002/anie.202213927**.

25 Q. Zhao, Y. Yang, G. Xiong, J. Chen, T. Xu, Q. Xu, R. Zhang, W. Yao, H. Li and C.-S. Lee, Calcium Single Atom Confined in Nitrogen-Doped Carbon-Coupled Polyvinylidene Fluoride Membrane for High-Performance Piezocatalysis, *J. Am. Chem. Soc.*, 2024, **146**(24), 16648–16658, DOI: **10.1021/jacs.4c03851**.

26 Q. Zhu, X. Song, X. Chen, D. Li, X. Tang, J. Chen, Q. Yuan and A. High, Performance Nanocellulose-PVDF Based Piezoelectric Nanogenerator Based on the Highly Active CNF@ZnO via Electrospinning Technology, *Nano Energy*, 2024, **127**, 109741, DOI: **10.1016/j.nanoen.2024.109741**.

27 Z. Shao, X. Zhang, Z. Song, J. Liu, X. Liu and C. Zhang, Simulation Guided Coaxial Electrospinning of Polyvinylidene Fluoride Hollow Fibers with Tailored Piezoelectric Performance, *Small*, 2023, **19**(38), 2303285, DOI: **10.1002/smll.202303285**.

28 S. Wang, W. Tong, Y. Li, P. Zhang, Y. Liu, Y. Chen and Y. Zhang, Contributions of Piezoelectricity and Triboelectricity to a Hydroxyapatite/PVDF–HFP Fiber-film Nanogenerator, *Nano Energy*, 2023, **105**, 108026, DOI: **10.1016/j.nanoen.2022.108026**.

29 Z. Shao, X. Zhang, J. Liu, X. Liu and C. Zhang, Electrospinning of Highly Bi-Oriented Flexible Piezoelectric Nanofibers for Anisotropic-Responsive Intelligent Sensing, *Small Methods*, 2023, **7**(9), 2300701, DOI: **10.1002/smtd.202300701**.

30 M.-Y. Qian, C.-H. He and J.-H. He, Enhanced Piezoelectric Performance of PVDF Nanofibers by Biomimicking the Spider's Long Liquid Transport, *Chem. Eng. J.*, 2024, **483**, 149159, DOI: **10.1016/j.cej.2024.149159**.

31 J.-H. Zhao, B.-S. He, A.-S. Li, C.-N. Wang, Q.-Q. Li and Z.-J. Hu, Polar Phase Formation and Piezoelectricity of PVDF by Hot-pressing under Electrostatic Intermolecular Interactions, *Chin. J. Polym. Sci.*, 2022, **40**, 799–806, DOI: **10.1007/s10118-022-2706-4**.

32 Y. Liu, W. Tong, L. Wang, P. Zhang, J. Zhang, X. Wang, S. Zhang, Y. Liu, S. Liu, S. Wang, M. Chai and Y. Zhang, Phase Separation of a PVDF–HFP Film on an Ice Substrate to Achieve Self-polarisation Alignment, *Nano Energy*, 2023, **106**, 108082, DOI: **10.1016/j.nanoen.2022.108082**.

33 T. Li, M. Qu, C. Carlos, L. Gu, F. Jin, T. Yuan, X. Wu, J. Xiao, T. Wang, W. Dong, X. Wang and Z.-Q. Feng, High-Performance Poly(vinylidene difluoride)/Dopamine Core/Shell Piezoelectric Nanofiber and Its Application for Biomedical Sensors, *Adv. Mater.*, 2020, **33**(3), 2006093, DOI: **10.1002/adma.202006093**.

34 T. Li, F. Jin, M. Qu, F. Yang, J. Zhang, T. Yuan, W. Dong, J. Zheng, T. Wang and Z.-Q. Feng, Power Generation from Moisture Fluctuations Using Polyvinyl Alcohol-Wrapped Dopamine/Polyvinylidene Difluoride Nanofibers, *Small*, 2021, **17**(36), 2102550, DOI: **10.1002/smll.202102550**.

35 Z. Qiu, T. Lei, S. Li, X. Cai and K. Yang, Insights into Polymorphic Transition of PVDF during Nonsolvent-Induced Phase Separation, *Macromolecules*, 2024, **57**(3), 1159–1168, DOI: **10.1021/acs.macromol.3c02394**.

36 A. Park, J.-Y. Jung, S. Kim, W. J. Kim, M. Y. Seo, S. Kim, Y. J. Kim and W. B. Lee, Crystallization Behavior of Polyvinylidene Fluoride (PVDF) in NMP/DMF Solvents: A Molecular Dynamics Study, *RSC Adv.*, 2023, **13**(19), 12917–12924, DOI: **10.1039/D3RA00549F**.

37 I. Priyan Shanura Fernando, W. W. Lee, E. J. Han and G. Ahn, Alginate-based Nanomaterials: Fabrication Techniques, Properties, and Applications, *Chem. Eng. J.*, 2020, **391**, 123823, DOI: **10.1016/j.cej.2019.123823**.

38 L. Liu, W. Fu, L. Wang, H. Tian and X. Shan, Piezoelectricity of PVDF Composite Film Doped with Dopamine Coated Nano-TiO2, *J. Alloys Compd.*, 2021, **885**, 160829, DOI: **10.1016/j.jallcom.2021.160829**.

39 X. Kong, Q.-Z. Wang, F.-Q. Kou, X. Wu, J. Zhao, H.-M. Huo, D.-E. Zhang, L. Hao and Y.-J. Chang, Study on The Effect of The Ion-dipole Interactions on The Polymorphism Regulation and Filtration Performance of PVDF Membranes, *J. Ind. Eng. Chem.*, 2024, **138**, 200–207, DOI: **10.1016/j.jiec.2024.03.053**.

40 Z. Cui, N. T. Hassankiadeh, Y. Zhuang, E. Drioli and Y. M. Lee, Crystalline Polymorphism in Poly(vinylidenefluoride) Membranes, *Prog. Polym. Sci.*, 2015, **51**, 94–126, DOI: **10.1016/j.progpolymsci.2015.07.007**.

41 Y.-Z. Huang, Z. Liu, L.-W. Li, H.-Z. He, Z. L. Wang, J.-P. Qu, X. Chen and Z.-X. Huang, Giant Piezoelectric Coefficient of Polyvinylidene Fluoride with Rationally Engineered Ultra-fine Domains Achieved by Rapid Freezing Processing, *Adv. Mater.*, 2024, 2412344, DOI: **10.1002/adma.202412344**.

42 H. Watarai and T. Sakamoto, Satoshi Tsukahara, In Situ Measurement of Dielectrophoretic Mobility of Single Polystyrene Microparticles, *Langmuir*, 1997, **13**(8), 2417–2420, DOI: **10.1021/la961057v**.

43 S. Mhatre, Dielectrophoretic Motion and Deformation of a Liquid Drop in an Axisymmetric Non-uniform AC Electric Field, *Sens. Actuators, B*, 2017, **239**, 1098–1108, DOI: **10.1016/j.snb.2016.08.059**.